Bioactive Materials 44 (2025) 220–235

Contents lists available at ScienceDirect

Bioactive Materials

journal homepage: www.keaipublishing.com/en/journals/bioactive-materials

Injectable acellular matrix microgel assembly with stem cell recruitment and chondrogenic differentiation functions promotes microfracture-based articular cartilage regeneration

Junlin Chen [a,b,c,d], Qingtao Li [b,c,d,e], Haofei Li [a,b,c], Chuhan Lv [a,b,d], Hongbo Yu [a,b,c], Qi Feng [a,b,c], Hua Dong [a,b,c,d,*]

[a] School of Materials Science and Engineering, South China University of Technology, Guangzhou, 510641, China
[b] National Engineering Research Center for Tissue Restoration and Reconstruction (NERC-TRR), Guangzhou, 510006, China
[c] Key Laboratory of Biomedical Materials and Engineering of the Ministry of Education, South China University of Technology, Guangzhou, 510641, China
[d] Guangdong Province Key Laboratory of Biomedical Engineering, South China University of Technology, Guangzhou, 510641, China
[e] School of Medicine, South China University of Technology, Guangzhou, 510006, China

ARTICLE INFO

Keywords:
Cartilage repair and regeneration
Cartilage acellular matrix
Injectable microgel assembly
BMSCs recruitment
Microfracture
Chondrogenic differentiation

ABSTRACT

Articular cartilage repair and regeneration is still a significant challenge despite years of research. Although microfracture techniques are commonly used in clinical practice, the newborn cartilage is usually fibrocartilage rather than hyaline cartilage, which is mainly attributed to the inadequate microenvironment for effectively recruiting, anchoring, and inducing bone marrow mesenchymal stem cells (BMSCs) to differentiate into hyaline cartilage. This paper introduces a novel cartilage acellular matrix (CACM) microgel assembly with excellent microporosity, injectability, tissue adhesion, BMSCs recruitment and chondrogenic differentiation capabilities to improve the microfracture-based articular cartilage regeneration. Specifically, the sustained release of simvastatin (SIM) from the SIM@CACM microgel assembly efficiently recruits BMSCs in the early stage of cartilage regeneration, while the abundant interconnected micropores and high specific area assure the quick adhesion, proliferation and infiltration of BMSCs. Additionally, the active factors within the CACM matrix, appropriate mechanical properties of the microgel assembly, and excellent tissue adhesion provide a conductive environment for the continuous chondrogenic differentiation of BMSCs into hyaline cartilage. Owing to the synergistic effect of the above-mentioned factors, good articular cartilage repair and regeneration is achieved.

1. Introduction

Articular cartilage is a crucial connective tissue with the main functions of bearing loads, lubricating joints, and buffering external forces [1,2]. However, the population aging, daily abrasion, acute trauma or chronic diseases often lead to its damage or degeneration, causing joint pain, motor dysfunction, and osteoarthritis [3,4]. Due to the lack of blood vessels, nerves, and lymphatic tissue, articular cartilage shows limited self-repair and regenerative ability. At present, the clinic treatments for articular cartilage defect include microfracture, allogeneic transplantation, autologous cartilage implantation, and autologous chondrocyte implantation [5], among which microfracture is adopted as the gold standard and first-line therapy for cartilage repair owing to its low cost, good short-term curative effect and simple operation [6,7]. After drilling tiny holes in the subchondral plate via microfracture operation, blood and a few BMSCs exuded from the bone marrow cavity form clot in the cartilage defect and thereby alleviate pain in the short term, but the newborn fibrocartilage in defect site is quite different from natural hyaline cartilage, resulting in poor long-term repairing effects [8–10]. This is mainly attributed to the deficiency of *in vivo* microenvironment (including biochemical cues and mechanical support) for recruiting, anchoring, and inducing BMSCs to differentiate into hyaline

Peer review under responsibility of KeAi Communications Co., Ltd.
* Corresponding author. School of Materials Science and Engineering, South China University of Technology, Guangzhou, 510641, China.
E-mail addresses: junlinchencjl@163.com (J. Chen), mcqtli@scut.edu.cn (Q. Li), lihaofei1192@163.com (H. Li), lvchu0510@163.com (C. Lv), 15897682305@163.com (H. Yu), feng2119@scut.edu.cn (Q. Feng), donghua@scut.edu.cn (H. Dong).

https://doi.org/10.1016/j.bioactmat.2024.10.013
Received 7 August 2024; Received in revised form 29 September 2024; Accepted 14 October 2024

cartilage [11–13].

Acellular matrix is very attractive as raw materials for tissue engineering and regenerative medicine because of its fantastic biocompatibility and abundant biochemical cues like growth factors [14,15]. Traditional acellular matrix-based scaffolds, such as freeze-dried or 3D-printed porous scaffolds, bulky hydrogels and injectable hydrogels, have their own shortcomings [16–19]. For example, freeze-dried or 3D-printed porous scaffolds as well as bulky hydrogels are not suitable for minimally invasive surgery and their dimensions usually don't match well with irregular cartilage defect even after elaborate shaping during surgery [20,21]. In contrast, injectable hydrogels can address the above problems but cells cannot infiltrate after adhering onto the injectable hydrogel surface due to the lack of internal micropores and thus restrict severely the cartilage regeneration [22–24]. In recent years, the emergency of microgels (micro-sized hydrogels) provides a new approach to construct scaffolds while still maintains their injectability [25–27]. Compared to injectable hydrogels, the small size and high specific surface area of microgels greatly enhance the nutrient transportation [28,29]. More importantly, microgel assembly can be further constructed using assembling agent, providing 3D mechanical support for cell adhesion, proliferation and differentiation [30–32]. The interconnected micropores in microgel assembly benefit cell infiltration and tissue formation before microgel degradation, both of which promote cell survival and tissue regeneration [33–35].

In this paper, we report a novel strategy to improve the cartilage repair and regeneration effect of microfracture. Specifically, herein we construct an injectable cartilage acellular matrix (CACM) microgel assembly with BMSCs recruitment and chondrogenic differentiation functions that can be easily integrated with microfracture operation (Scheme 1). To reinforce the BMSCs recruitment from the bone marrow cavity, SIM, a non-protein small molecular drug approved by Food and Drug Administration (FDA) [36,37], is encapsulated in CACM microgels. The as-prepared microgels are then assembled into injectable microgel assembly (labelled as SIM@CACM microgel assembly) via dynamic Schiff base bonds after the addition of oxidized sodium alginate (OSA). Upon injecting into the articular cartilage defect after microfracture surgery, SIM@CACM microgel assembly can recruit BMSCs via sustained release of SIM, enhance their residency by offering numerous anchoring sites inside the porous 3D construct and induce their chondrogenic differentiation via the stimuli of biomechanical and biochemical cues. As a consequence, newborn hyaline cartilage rather than fibrocartilage can be formed in defect site. Compared with other traditional chondrocyte induction methods, SIM@CACM microgel assembly recruits endogenous BMSCs through the sustained release of SIM and thus eliminates the need for exogenous cell sources and the resulting immune rejection. Its highly porous 3D structure and high specific surface area ensure rapid cell adhesion, proliferation and infiltration. The ECM-like microenvironment (abundant active factors and suitable mechanical strength) promote chondrogenic differentiation of BMSCs. Furthermore, unlike bulky hydrogels or solid scaffolds that require invasive procedures and are difficult to match irregular defects, SIM@CACM microgel assembly is injectable, allowing for minimally invasive treatment and precise filling of defect sites. We believe our strategy, i.e., the combination between SIM@CACM microgel assembly and microfracture, provides a promising solution to cartilage repair and regeneration.

2. Materials and methods

2.1. Materials

Simvastatin (SIM), trypsin, deoxyribonuclease, ribonuclease A, hexane, span 80, 1-(3-Dimethylaminopropyl)-3-ethylcarbodiimide (EDC), N-Hydroxy succinimide (NHS), sodium alginate, and sodium periodate were purchased from Sigma (Germany). NaOH, tris (Hydroxymethyl) aminomethane hydrochloride (Tris-HCL), type II collagenase, Triton X-100, rat blood and ethanol anhydrous were obtained from Macklin (China).

2.2. Preparation and characterization of CACM

CACM was prepared by a modified chemical and physical method reported in previous work [38]. In brief, cartilage pieces were cut off from the porcine knee, washed thoroughly and decellularized via 3 cycles of repeated freezing and thawing from −80 °C to 26 °C. Place the cartilage pieces into purified water and use a tissue homogenizer (Waring, USA) to break them into 2–3 mm fragments, followed by 3 min of sonication. Centrifuge the suspension at 1500 rpm for 10 min and discard the supernatant. Add ultrapure water, sonicate for another 3 min, and centrifuge at 3000 rpm for 10 min. Discard the supernatant and collect the precipitate. To realize virus inactivation, the as-prepared cartilage pieces were immersed in 2 wt% NaOH solution for 2 h,

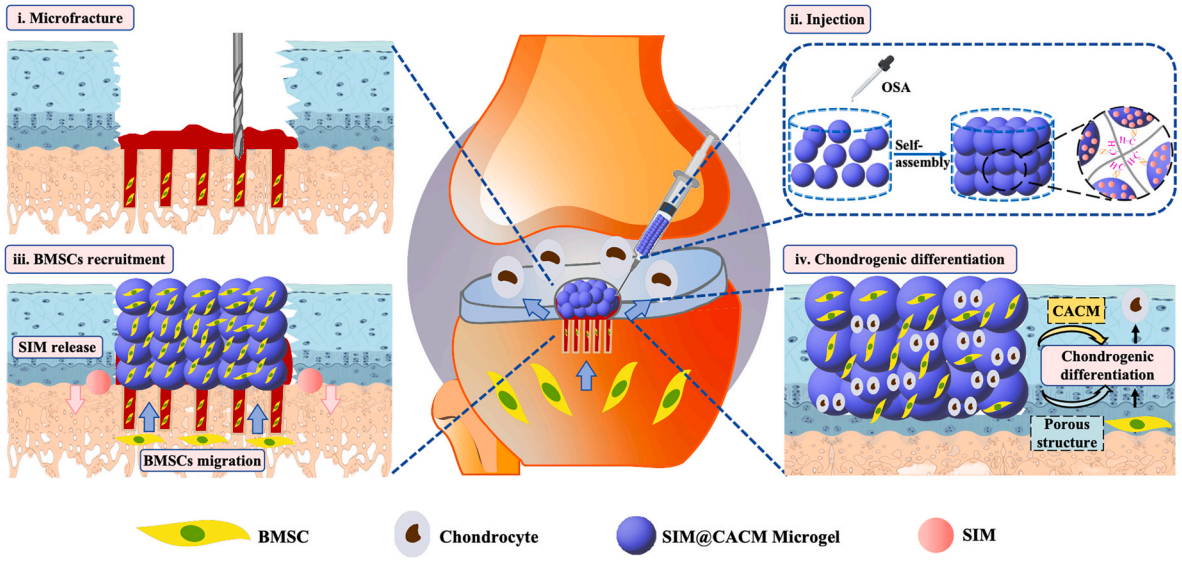

Scheme 1. Injectable SIM@CACM microgel assembly with BMSCs recruitment and chondrogenic differentiation functions promotes microfracture-based articular cartilage regeneration. This process incudes: (i) cleaning the cartilage defect and performing microfracture surgery; (ii) injecting SIM@CACM microgel assembly; (iii) releasing SIM and recruiting BMSCs from bone marrow cavity; (iv) inducing the chondrogenic differentiation of BMSCs.

rinsed with deionized water, treated with 0.5 % trypsin for 24 h (replaced with fresh trypsin every 4 h) and finally soaked in nuclease solution (containing 50 U/mL deoxyribonuclease and 1 U/mL ribonuclease A in 10 mM Tris-HCL, pH = 7.5) for 4 h. The residual enzyme was removed by treating cartilage pieces with 10 mM Tris-HCL (containing 10 U/mL peptidase) for 20 h and then PBS solution containing 1 % (v/v) Triton X-100 for 24 h. After soaking 6 times in PBS buffer (each time for 2h), CACM was harvested by lyophilization. All protocols were performed at 37 °C with constant shaking.

To confirm the cell removal from CACM, DNA concentration was quantified via the genome DNA purification kit (Thermo Scientific, USA). The procedure involved digesting CACM with the provided lysate, followed by emulsification with chloroform. After centrifugation, the supernatant was discarded and DNA was precipitated using a DNA precipitation solution. The precipitated DNA was dissolved in sterile deionized water again after multiple rinsing and purification steps. DNA quantification was performed three times using a NanoDrop 2000 (Thermo Scientific, USA) and results were normalized to the original dry weight of the samples. Additionally, the total glycosaminoglycans (GAGs) content was measured using a dimethylmethylene blue (DMMB) colorimetric quantitative assay kit (GENMED, USA). CACM was finely chopped and enzymatically digested using a papain extraction reagent (Sigma, Germany) at 65 °C for 18 h. The soluble GAGs concentration was determined according to the protocol of the kit, and the standard curve of GAGs was used to correlate with the dry weight of the CACM. Moreover, hydroxyproline, a key collagen type II (Col II) component, was quantified using a hydroxyproline assay kit (Solarbio, China). CACM was minced into 1 mm^2 pieces, and the resultant supernatant was analyzed to measure the hydroxyproline content, which was then converted to Col II content using a formula provided in the kit instructions.

To evaluate the immunogenicity of CACM, six healthy New Zealand rabbits were anesthetized, and their dorsal area was shaved and disinfected. Four incisions (2 cm) were made symmetrically on both sides of the spine to create subcutaneous pockets for CACM implants (3 wt% of CACM precursor cross-linked through EDC-NHS solution). Each rabbit received four implants (two on each side of the spine), and the skin is sutured. After 7 days, the rabbits were euthanized, and the implanted tissues were collected. The samples were fixed in 4 % of paraformaldehyde, followed by paraffin embedding and sectioning into 5 μm slices. Hematoxylin and eosin (H&E) staining was performed to evaluate inflammatory responses.

2.3. Preparation and characterization of SIM@CACM microgels

3 wt% of CACM precursor was prepared and its pH value was adjusted to 7.0, followed by the addition of SIM solution. The SIM@CACM microgels were produced using an emulsion dispersion method. Hexane containing 5 wt% of Span 80 was used as the oil phase and the water-to-oil ratio was set as 1:5 (v/v). In brief, the mixed precursor was incrementally injected into the oil phase under magnetic stirring, stirred at 6000 rpm for 30 min at 37 °C. Subsequently, 2 mL of EDC-NHS solution (dissolved in 95 % ethanol), serving as the crosslinking agent, was rapidly injected into the emulsion and stirred continuously for 6 h.

After demulsification using anhydrous ethanol, the SIM@CACM microgels were separated by centrifugation and washed with anhydrous ethanol for three times. Finally, the microgels were dispersed in deionized water and stored at 4 °C. The same procedure was applied to fabricate pure CACM microgels as a control group. The functional groups of SIM, CACM and SIM@CACM microgels were identified using a Bruker Tensor 27 FTIR spectrometer (Nicolet IS5, Germany) under the reflectance mode. All spectra were recorded between 4000 and 500 cm^{-1} with a resolution of 1 cm^{-1}. Microgels were photographed with a bright-field microscopy (Thermo Scientific, USA) and their size was measured using Image J software.

2.4. Synthesis of OSA

2g of sodium alginate was dissolved in 100 mL of deionized water and stirred until it was fully dissolved. 3g of sodium periodate dissolved in 30 mL of deionized water was then added into the sodium alginate solution and stirred for 6 h at room temperature. Thereafter, 2 mL of ethylene glycol was dropped into the solution and continuously stirred for 30 min to completely terminate the reaction. Finally, the solution was dialyzed for 2 days (MWCO = 8000–10000) and OSA was obtained by lyophilization.

2.5. Fabrication and component optimization of SIM@CACM microgel assembly

The OSA concentration used for fabrication of SIM@CACM microgel assembly was identified by the adhesion and wear resistance test. Specifically, 50 μL of OSA solution with different concentrations (10, 20 and 30 wt%) were added to 1 mL of SIM@CACM microgels and gently stirred until microgel assembly was formed. A cartilage defect model was established *in vitro* using rabbit joints. SIM@CACM microgel assembly was then filled into the defect, washed with PBS through a syringe. When the SIM@CACM microgel assembly cannot be washed off the cartilage defect, the corresponding OSA concentration was fixed for the following experiments.

SIM concentration in SIM@CACM microgel assembly was optimized via BMSCs viability and recruitment efficiency. Specifically, BMSCs with a density of 2×10^4 mL^{-1} were co-cultured with SIM@CACM microgel assembly fabricated under different SIM concentrations (1, 3 and 6 mg/mL). BMSCs were then stained with live/dead dye solution for 30 min at room temperature after co-culture for 1, 3 and 5 days and observed by confocal laser scanning microscopy (CLSM, Leica, Germany). Cell proliferation was measured by CCK-8 assay, i.e., microgels were treated with 10 % of CCK-8 solution (GLPBIO, USA) for 1h and the absorbance values (OD) at 450 nm were detected using a spectral scanning multimode reader (Thermo Scientific, USA). To assess the recruitment efficiency of SIM@CACM microgel assembly on BMSCs, the chemotaxis assay was performed using the Transwell system (Corning, USA). Briefly, the upper chamber was seeded with BMSCs (5×10^4 mL^{-1}). SIM@CACM microgel assembly with three SIM concentrations were added to the lower chamber. The culture medium containing 10 % serum was injected into the upper and lower chambers. After incubation for 24 h, BMSCs on the back of the membrane in upper chamber were fixed and stained with 0.5 % of crystal violet dye (Sigma, Germany). After removing the non-migrated cells with a cotton swab, the migrated cells were imaged and counted using bright-field microscopy (Thermo Scientific, USA) to determine the optimal SIM concentration.

In addition, wound healing assay was further carried out using a transwell system (0.4 μm, Corning, USA). To eliminate the influence of BMSC proliferation, serum-free culture medium was used for this experiment. Briefly, BMSCs (5×10^4 mL^{-1}) were cultured in the lower chamber of a 24-well plate until reaching 70–80 % confluence. A straight scratch was gently made at the center of the well using a 200 μL pipette. Prior to adding the SIM@CACM microgel assembly to the upper chamber, exfoliated cells were washed away with PBS. Scratch closure was observed at 0, 6, 12 and 24 h using a bright-field microscopy (Thermo Scientific, USA), and the scratch area and percentage of repair were quantified using ImageJ software (n = 3).

2.6. Physicochemical characterization of SIM@CACM microgel assembly

SIM release from SIM@CACM microgel assembly was assessed as follows: 1 mL of SIM@CACM microgel assembly was injected into the upper chamber of a 6-well transwell (Corning, 0.4 μm) and spread over the bottom of the well. Then 2 mL of PBS was added to the lower chamber of the transwell. The whole transwell was placed under constant shaking of 30 rpm at 37 °C. The supernatant was collected and

replaced with the same volume of fresh PBS every 2 days until day 20. The UV–visible spectra of the supernatants were recorded in the wavelength range of 500 to 200 nm using a spectrophotometer (Cary 60 UV, Agilent, Singapore). The concentrations of released SIM at different time points were determined by the standard calibration curve that was plotted using different SIM concentrations and the peak height at 238 nm.

The rheological properties of SIM@CACM microgels and microgel assembly were investigated through a rheometer (AR 2000, TA Instruments) with a parallel plate configuration (plate diameter: 50 mm). Compressive moduli of SIM@CACM microgels and microgel assembly before/after injection and their tensile moduli after adhesion onto pigskin were measured (n = 4 per group) using a dynamic mechanical analyser (DMA Q800, USA).

Biodegradability was assessed through *in vitro* experiments according to the literature [39]. Briefly, SIM@CACM microgel assembly were incubated in 2 mL of PBS containing 1 ng/mL of type II collagenase at 37 °C and 5 % CO_2 using a humidified shaker incubator. The enzyme solution was replaced once a day. After drying, the weight of each sample was measured using a high-precision electronic balance. The initial weight was recorded as W_0, and the weight of the degraded assembly as Wn. The degradation rate (%) was calculated using the formula:

$$degradation\ rate\ (\%) = \frac{W_0 - W_n}{W_0} \times 100\%$$

To evaluate the stability in blood, SIM@CACM microgel assembly was placed in a Petri dish, soaked in blood, and incubated at 37 °C under shaking for 24 h. Hemocompatibility was evaluated as follows. Anticoagulated whole blood was centrifuged at 3000 rpm for 10 min and washed three times with PBS to isolate red blood cells (RBCs). These RBCs were then diluted fivefold in PBS. 1 mL of RBC suspension was incubated with different volumes (50, 100, and 150 μL) of SIM@CACM microgel assembly at 37 °C for 3 h. After incubation, the samples were centrifuged at 1000 rpm for 10 min, and the absorbance of supernatant was measured at 545 nm using a microplate reader (Tecan, Switzerland). RBCs treated with deionized water were used as a positive control, while untreated RBCs served as a negative control. The hemolysis rate was calculated using a specified formula.

$$Hemolysis(\%) = \frac{\left[OD_{sample} - OD_{negative\ controls}\right]}{\left[OD_{positive\ controls} - OD_{negative\ controls}\right]} \times 100\ \%$$

The porous structure of SIM@CACM microgel assembly was characterized by field emission scanning electron microscopy (FESEM, Carl Zeiss Merlin, Germany) and CLSM. Prior to CLSM test, the SIM@CACM microgels were first stained with FITC-labelled isothiocyanate, assembled at 37°C and finally observed via CLSM.

2.7. BMSC adhesion and infiltration in SIM@CACM microgel assembly

BMSC adhesion and infiltration behaviors in the SIM@CACM microgel assembly were explored as follows: 0.2 mL of CACM hydrogel and SIM@CACM microgel assembly were placed in a circular mold respectively. BMSCs (5×10^4 mL^{-1}) were seeded on their surface and incubated for 1, 3 and 5 days. BMSC infiltration distance was then measured by CLSM after staining with calcium chlorophyll AM.

2.8. In vitro chondrogenic differentiation and chondrosphere assay of BMSCs

To evaluate the effect of SIM@CACM microgel assembly on the chondrogenic differentiation of BMSCs, CACM microgel assembly, SIM@CACM microgel assembly and CACM hydrogel were placed in 24-well plates respectively and co-cultured with BMSCs (2×10^5 mL^{-1}). After 24 h of culture using complete culture medium, the culture medium was replaced with fresh chondrogenic differentiation medium and the chondrogenic culture was continued for another 2 weeks. Subsequently, GAGs content was measured by Alcian blue method. In short, BMSCs were fixed, washed twice with PBS, and then stained with 1 % of Alcian blue (Sigma, Germany) for 30 min at room temperature. The Col II expression was evaluated by immunofluorescence. Specifically, cells were fixed, blocked with 2 % BSA/PBS, and labelled in turn with rabbit polyclonal anti-Col II antibody (Servicebio, China) overnight at 4 °C, FITC-conjugated phospholipid-like protein (Servicebio, China) and DAPI (Servicebio, China). Finally, CLSM was used to analyze the samples, and the fluorescence intensity were measured using Image J software (n = 4).

In order to further study the ability of cartilage formation and differentiation of SIM@CACM microgel assembly and simulate its three-dimensional relationship with cells *in vivo*, SIM@CACM microgel assembly and microgels were placed at the bottom of 10 mL centrifuge tube. Then, 1 mL of BMSCs suspension with the concentration of 3×10^5 $mL^{-1}$was added and cultured in chondrogenic differentiation medium for 4 weeks at 37°C. BMSCs clusters were centrifuged to the bottom of tube as the control group, and cultured with the same medium. Quantitative real-time polymerase chain reaction (qRT-PCR) was carried out according to the manufacturer's scheme. Total RNA was extracted from the samples (n = 4) using Trizol (Thermo Scientific, USA) and quantified using NanoDrop 2000 (Thermo Scientific, USA). The expressions of genes involved in cartilage development such as type II collagen (Col 2a1), aggrecan (Acan), type I collagen (Col 1a1), and SRY box 9 (Sox 9), were assessed by first-strand cDNA synthesis using oligoadaptor primers and AMV reverse transcriptase (TAKARA, Tokyo, Japan). All gene expression data were normalized to glyceraldehyde-3-phosphate dehydrogenase (GAPDH) and calculated using the $2^{-\Delta\Delta Ct}$ value method. The mouse specific primer sequences were given in Table S1. Immunohistochemical staining was performed by cutting paraffin-embedded samples into 5 μm sections, deparaffinizing in xylene, rehydrating in a graded series of ethanol solutions. In order to eliminate the activity of endogenous peroxidase, slices were incubated in methanol containing 3 % (v/v) hydrogen peroxide for 20 min. Antigen repair was carried out by steam treatment in 0.01 M sodium citrate buffer (pH 6.0) at 90–100 °C for 30 min. The samples were then blocked with 1 wt% of BSA for 30 min, incubated with primary antibodies against Col I (rabbit polyclonal anti-type I collagen, Sigma), Col II (rabbit polyclonal anti-type II collagen, Sigma) or aggrecan (mouse monoclonal anti-aggrecan, Abcam) at dilutions of 1:500, 1:500 and 1:100 respectively at 4 °C, secondary antibody (biotin-coupled goat anti-mouse/rabbit IgG) for 30 min, and streptavidin-biotin complex (SABC) for 30 min. The samples were finally visualized using 3, 3′-diaminobenzidine (DAB, Sigma, Germany) staining.

2.9. In vivo animal test

All animal experiments were conducted following the Public Health Service policies, the Animal Welfare Act, and the Laboratory Animal Committee (LAC) of South China University of Technology Policy on the Human Care and Use of Vertebrate Animals (SYXK 2017-0178).

In long-term cartilage repair experiments, twenty-four healthy New Zealand white rabbits (12 weeks, 2.5–3.0 kg) were randomly divided into four groups and anesthetized by intravenous injection of pentobarbital sodium (30 mg/kg body weight). Bilateral femoral defects with the size of 5 mm × 2 mm (diameter × height) were created in the distal metaphysics region using a dental drill, and manufacturing microfractures using a needle. The defects were then flushed with 0.9 % saline. CACM microgels, CACM microgel assembly and SIM@CACM microgel assembly were injected into these defects with a 1 mL syringe at room temperature (26 °C). For the *in vivo* cell recruitment experiment, 12 rabbits were divided into 3 groups, and the surgical process was the same as the long-term cartilage repair experiment. Two experimental groups were injected with CACM microgel assembly and SIM@CACM

microgel assembly. The surgical sites were then sutured and covered with sterile gauze. After surgery, the New Zealand rabbits were individually housed in cages and fed individually.

On the 5th day, the New Zealand rabbits were euthanized, and their femurs were taken out and fixed in 4 % of paraformaldehyde to observe cell recruitment *in vivo*. In weeks 4 and 8, the residual New Zealand rabbits were euthanized and the femurs were removed and fixed in 4 % of paraformaldehyde. Samples were extracted and decalcified with 12.5 % of ethylenediaminetetraacetic acid (EDTA), dehydrated in a series of graded alcohols and embedded in paraffin. Serial sections of the samples were stained with hematoxylin-eosin, safranin O-fast green and Col II (rabbit polyclonal anti-type II collagen, Abcam, UK) for microscopic observation. All animal experiments were approved by the Animal Experimentation Centre of the South China University of Technology in

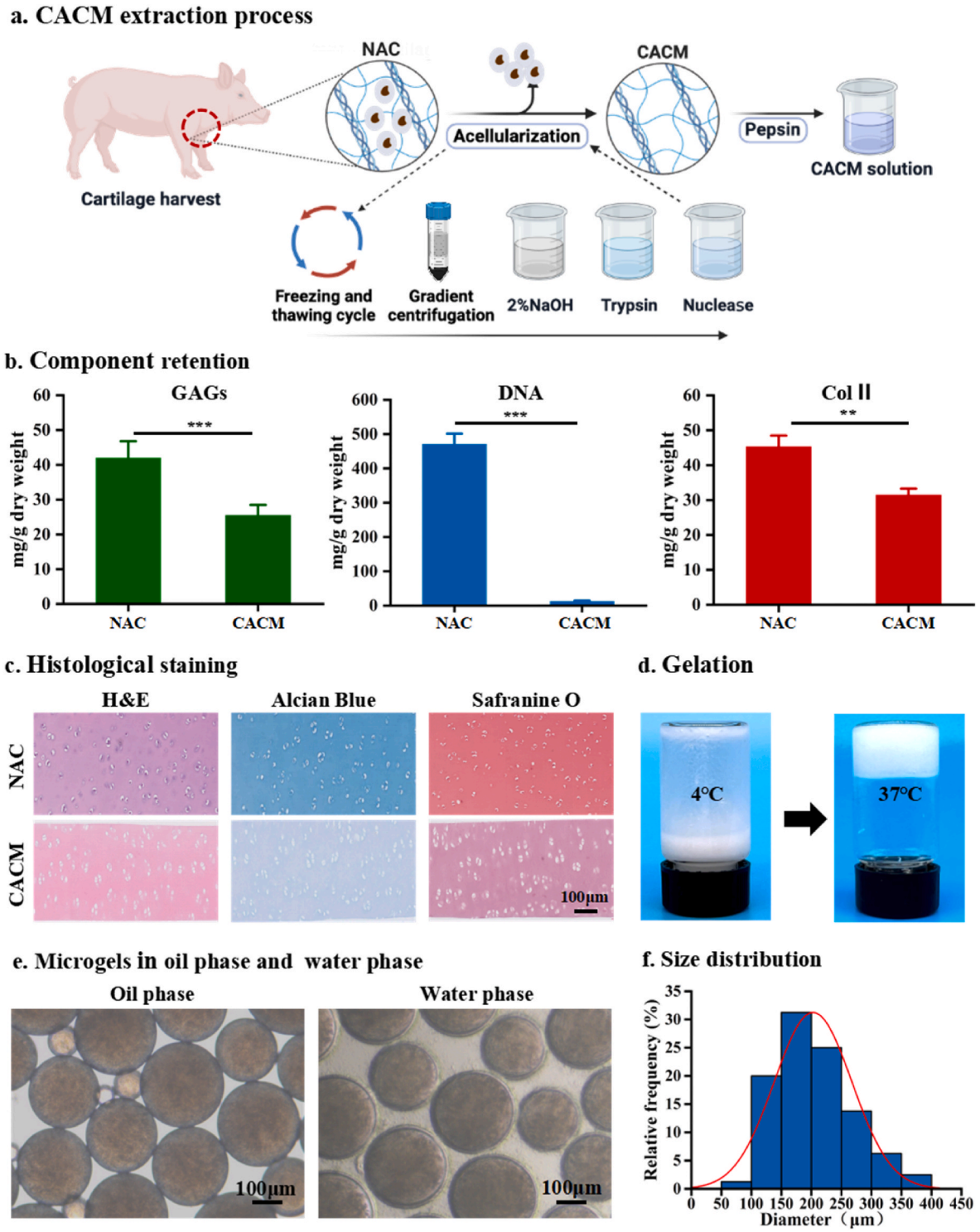

Fig. 1. Preparation and characterization of CACM and SIM@CACM microgel: a) schematic illustration on CACM extraction process from natural articular cartilage (NAC); b) GAGs, DNA and Col II retention of NAC and CACM; c) histological staining including H&E staining, Alcian blue staining and safranin O staining; d) optical images of CACM gelation; e) optical images of SIM@CACM microgels in oil phase and water phase; f) size distribution of SIM@CACM microgels in water phase. ***P < 0.001, **P < 0.01, n $= 4$.

accordance with the Regulations on the Administration of Laboratory Animals. In order to quantitatively evaluate the curative effects of cartilage repair including the main tissue types, structural characteristics and cell-free degeneration changes, The ICRS scoring system (Table S2) and O 'Driscoll scoring system (Table S3) was used [66]. Scoring was performed in a blinded fashion by three independent observers.

2.10. Statistical analysis

One-way analysis of variance (ANOVA) was applied to calculate the differences between values, and all data were expressed as the mean ± standard deviation (SD). A value of $p < 0.05$ was considered statistically significant, and ns, *, **, *** represent $p > 0.05$, $p < 0.01$, $p < 0.001$, respectively.

3. Results and discussion

3.1. Preparation of CACM and SIM@CACM microgel

CACM was extracted from porcine articular cartilage according to a modified procedure shown in Fig. 1a. In our study, three kinds of CACMs were prepared by adjusting the treatment time of trypsin and Triton X-100 (Fig. S1a, supporting information), and the optimal acellularization process was determined by evaluating the DNA and Col II contents in CACM and the inflammatory response of subcutaneous implantation. As can be found in Fig. S1b, Col II content of the CACM treated with trypsin and Tritonx-100 for 24 h doesn't show obvious change while the DNA content decreases significantly, compared to those of the other two samples. H&E staining in Fig. S2 reveals that less inflammatory cells are found on the surface of CACM treated for 24h after subcutaneous implantation for 7 days compared with CACM treated for 6h, suggesting that the treatment by trypsin and Triton X-100 for 24h not only reduces DNA residues but also lowers the immunogenicity of CACM. If not specified, CACM with the lowest DNA content is used for the following experiments. Fig. 1b compares the GAGs, DNA and Col II contents between natural articular cartilage (NAC) and CACM. The DNA content decreases from 470.8 ± 30.6 ng/mg to 12.5 ± 2.4 ng/mg after acellularization of NAC, which is lower than the current commercial standard of 50 ng/mg for animal-derived biomaterials [40], and the DNA removal rate reaches 99.96 %. Meanwhile, the GAGs and Col II contents of NAC are 42.7 ± 5.3 mg/g and 45.3 ± 4.5 mg/g, and the corresponding values of CACM fall to 25.5 ± 3.0 mg/g and 31.5 ± 1.8 mg/g. The effect of acellularization was further verified using histological staining in Fig. 1c. H&E staining shows that nuclear cell structure of normal chondrocytes can be observed in NAC whilst only empty cartilage cavities are seen in CACM, indicating the disappearance of chondrocytes from CACM. Alcian blue and Safranine O staining reveal that CACM still maintain most of the polysaccharide sulfide and cartilage matrix. In addition, the as-obtained CACM also exhibits thermo-responsive behavior like cartilage extracellular matrix. As shown in Fig. 1d, CACM solution undergoes sol-gel transition when temperature rises from 4 °C to 37°C, possibly ascribed to the formation of triple helices in collagen at 37°C [41].

To ensure the fabrication of enough SIM@CACM microgels quickly, water-in-oil emulsion method instead of droplet-based microfluidics was used, followed by chemical crosslinking via amidation reaction (EDC/NHS). Fig. 1e gives the bright-field images of SIM@CACM microgels in the oil phase and water phase. As can be seen, these microgels show no obvious swelling after transferring from oil phase to water phase and their size is mainly distributed in the range of 100–250 μm. FTIR spectroscopy was used to confirm the presence of SIM and CACM in SIM@CACM microgels. In Fig. S3, the characteristic peaks of CACM at 1580 cm^{-1} (C-N stretching vibration and N-H bending vibration of aliphatic secondary amine, green dotted box) appears in SIM @CACM microgel powder. Meanwhile, the characteristic peaks of SIM at 2872 cm^{-1} and 2959 cm^{-1} (C-H stretching vibrations, yellow dotted frame) also shown in SIM@CACM microgel powder. This indicates that SIM has been successfully encapsulated in CACM microgels, and SIM@CACM microgels preserve the essential components of CACM [42–45].

3.2. Construction and characterization of SIM@CACM microgel assembly

OSA, as the microgel assembling agent, was synthesized by oxidation of sodium alginate using sodium periodate (Fig. 2a). Once adding into SIM@CACM microgels, the aldehyde groups of OSA can form Schiff base bonds with amino groups on SIM@CACM microgel surface. It can be seen from Fig. 2b that the as-formed SIM@CACM microgel assembly is semi-transparent and can be lifted by tweezers. Except for assembling microgels, the aldehyde groups of OSA also confers SIM@CACM microgel assembly with good tissue adhesion. Fig. 2c compares the tissue adhesion strength of SIM@CACM microgel assembly (dyed green) prepared under different OSA concentrations. Unassembled SIM@CACM microgels (0 % of OSA) are easily washed away by moderate flushing, implying their poor tissue adhesion towards cartilage defect. SIM@CACM microgel assembly obtained using 10 % and 20 % of OSA, however, can be partially washed off. In contrast, SIM@CACM microgel assembly with 30 % of OSA can withstand the moderate flushing and stick to the cartilage very well, indicative of its best tissue adhesion and mechanical strength (Movie S1). To ensure that the SIM@CACM microgel assembly won't fall off from the articular cartilage defect in subsequent animal test, 30 % of OSA is used to construct the microgel assembly.

In addition to OSA, SIM is also important in our material system. Compared with commonly used drugs for cell recruitment such as cytokines, SIM exhibits a much longer half-life within the physiological microenvironment and demonstrates good stability under various stimuli. Since the role of SIM is to recruit BMSCs, the optimal SIM concentration in SIM@CACM microgel assembly was determined via transwell cell migration experiment that mimics the BMSC migration from bone marrow cavity to cartilage defect (Fig. 2d). BMSCs were cultured on the upper surface of membrane within the transwell chamber, while SIM@CACM microgel assembly was placed in the lower petri-dish. Triggered by SIM release from the SIM@CACM microgel assembly, BMSCs migrate and penetrate through the porous membrane of transwell chamber. As shown in Fig. 2e and f, the best BMSC migration is achieved in SIM@CACM microgel assembly with 3 mg/mL of SIM. This indicates that such SIM@CACM microgel assembly has the strongest ability to induce BMSCs to migrate into the cartilage defect *in vivo* after microfracture [46,47]. Besides, the live-dead staining of BMSCs reveals that BMSC activity is not affected when SIM concentration is 1 mg/mL or 3 mg/mL, so the difference in transwell migration experiment is caused by the difference in SIM concentration. However, when SIM concentration reaches 6 mg/mL, BMSC growth is severely inhibited and the number of BMSCs is significantly less than the rest groups on day 5 (Fig. S4), suggesting that excessively high SIM concentrations can damage BMSC viability. Therefore, considering the cytocompatibility and BMSCs recruitment of SIM, 3 mg/mL of SIM (the SIM encapsulation efficiency is ~73–76 %, Fig. S5) is finally selected for use in subsequent experiments.

Besides, to further confirm the promotion of SIM with the optimal concentration on BMSC migration and the interaction between SIM@CACM microgel assembly and BMSCs within an isolated microenvironment, wound healing assay was employed using a transwell system where BMSCs were seeded in the lower chamber while SIM@CACM microgel assembly was placed in the upper chamber. The results in Fig. S6 demonstrate that BMSCs migration area and wound healing percentage in the SIM@CACM microgel assembly group were significantly higher than those in the other groups, indicating that SIM@CACM microgel assembly can enhance the migration ability of BMSCs by releasing SIM [48].

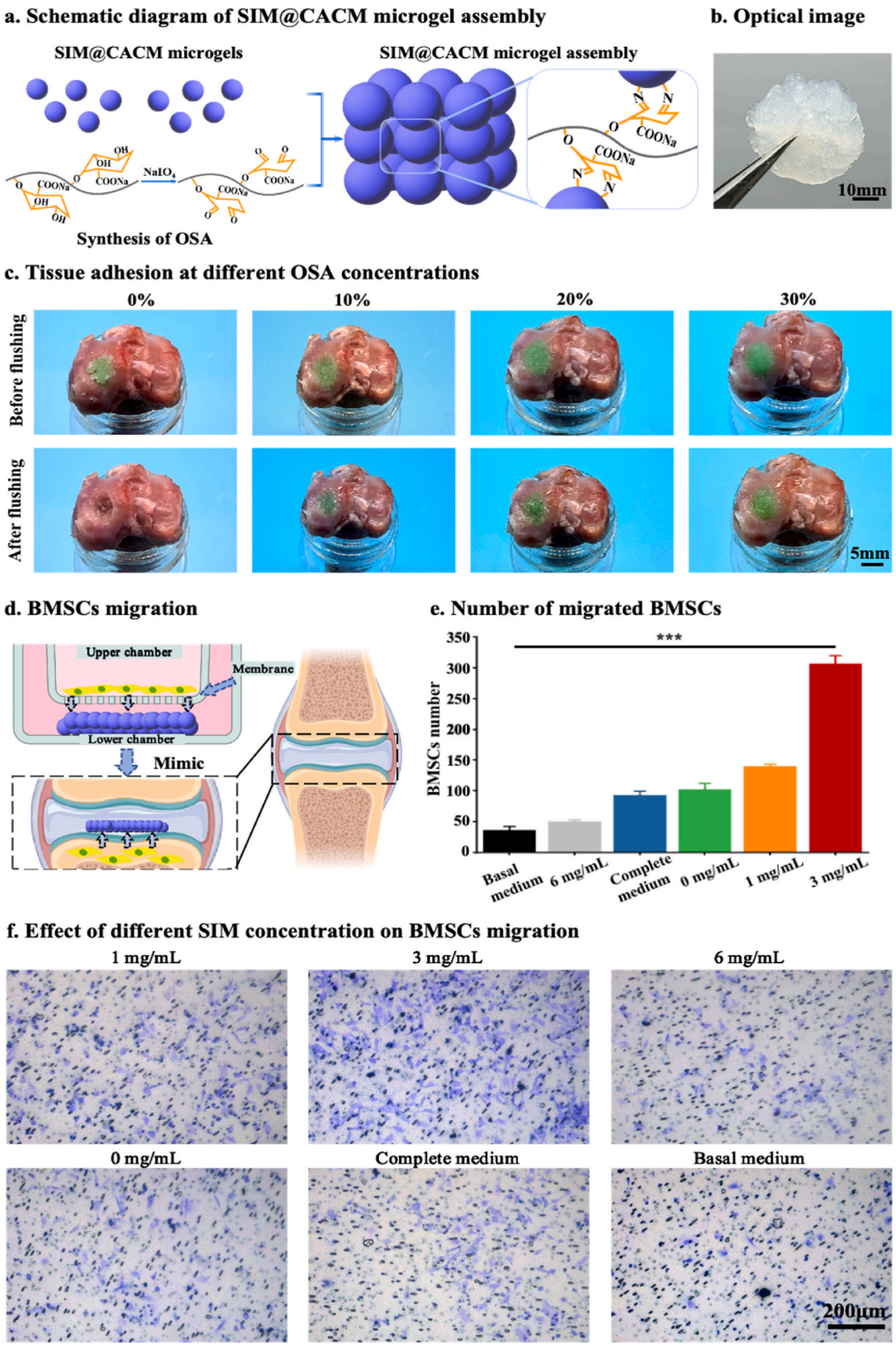

Fig. 2. Construction of SIM@CACM microgel assembly: a) schematic illustration on construction of SIM@CACM microgel assembly; b) optimal image of SIM@CACM microgel assembly; c) tissue adhesion strength of SIM@CACM microgel assembly obtained under different OSA concentrations; d) transwell migration experiment; e) the number of migrated BMSCs after crystal violet dye; f) bright-field photos of migrated BMSCs after crystal violet dye; ***$P < 0.001$, $n = 4$.

Fig. 3a lists *in vitro* SIM release curve of SIM@CACM microgel assembly. Interestingly, the sustained release speed of SIM is quite similar in the first 12 days and slows down dramatically thereafter, implying the BMSC recruitment might continue until day 12. Fig. 3b gives the compression curves of SIM@CACM microgels and SIM@CACM microgel assembly. Compared with the low compression modulus of the jammed SIM@CACM microgels (0.5 ± 0.1 kPa), SIM@CACM microgel assembly exhibits much higher compression modulus (11 ± 1.5 kPa), mainly ascribing to the dynamic crosslinking among microgels and thus offering appropriate mechanical cues for BMSC differentiation [49]. Meanwhile, the tissue adhesion strength was also quantitatively measured via tensile test of two pigskins stuck by SIM@CACM microgel assembly. It can be seen from Fig. 3c that the maximum tensile stress is 4 ± 0.4 kPa for pigskins stuck by SIM@CACM microgel assembly, which is significantly higher ($P < 0.001$) than the control group (pigskins stuck by jammed SIM@CACM microgels without OSA, 0.3 ± 0.1 kPa). Fig. 3d further compares their viscosity−shear rate behaviors. The viscosities of these two samples decrease with the increase of shear rate, indicative of their shear thinning properties. The higher viscosity of SIM@CACM microgel assembly (978 Pa s) at zero shear rate compared with jammed SIM@CACM microgels (217 Pa s) also confirms the important role of dynamic covalent bonds in the increase of viscosity. Oscillation amplitude sweep test in Fig. 3e shows that the storage moduli (G′) of two samples at low strain are higher than their respective loss modulus (G″), demonstrating their stable elasticity at low strain. With the increase of shear strain, a yield strain can be found where G″ starts to exceed G', and this suggests the sol–gel transition at high strain [50]. The yield strains are about 9 % for jammed SIM@CACM microgels, and change to 46 % for SIM@CACM microgel assembly, further proving the assembly performance. Since the Schiff base bonds between aldehyde groups and amino groups are dynamic, SIM@CACM microgel assembly also shows excellent self-healing property, which was proven via high low strain cycle experiments. The curves in Fig. 3f show reversible gel−sol transitions of SIM@CACM microgel assembly upon cyclic shearing at high strain (200 %) and low strain (1 %). At the strain of 200 %, G′ of SIM@CACM microgel assembly decreases from 600 Pa to 50 Pa, and is lower than G″, indicative of its sol state. On the contrary, when the strain becomes 1 %, G′ quickly recovers to around 600 Pa, which means that the SIM@CACM microgel assembly returns to the gel state. This repeated sol−gel transition demonstrates that SIM@CACM microgel assembly have excellent self-healing properties [51].

The injectability of SIM@CACM microgel assembly (dyed green) is

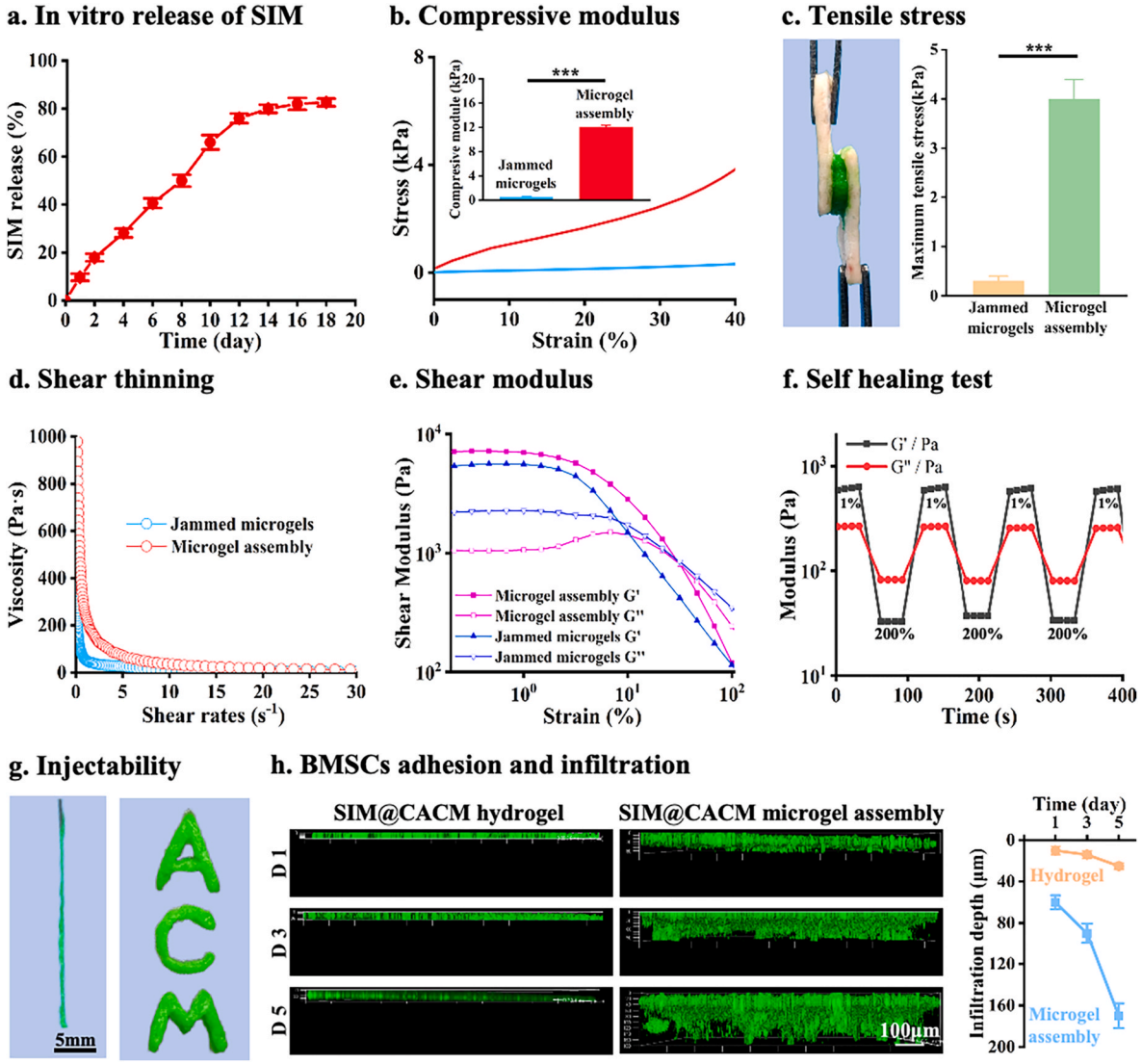

Fig. 3. Characterization of SIM@CACM microgel assembly: a) *in vitro* SIM release curve from SIM@CACM microgel assembly; b) compression test; c) tissue-adhesion test; d) shear thinning behavior; e) shear modulus of SIM@CACM microgel assembly; f) self-healing test; g) injectability of SIM@CACM microgel assembly; h) BMSC adhesion and infiltration inside SIM@CACM microgel assembly. ***$p < 0.001$, $n = 4$.

firstly demonstrated by its uniform extrusion through a small needle into arbitrary shapes, as shown in Fig. 3g. Movie S2 further illustrates the injection process of SIM@CACM microgel assembly into a cartilage defect, and its complete fillability in the defect site can be ascribed to its good injectability and tissue adhesion [52]. Note that the mechanical strength of SIM@CACM microgel assembly before and after injection doesn't show obvious difference (Fig. S7). Besides, SIM@CACM microgel assembly exhibits good stability in blood and excellent hemocompatibility without obvious hemolysis (Figs. S8 and S9). However, once immersing in a solution containing type II collagenase, it shows sound degradation, i.e., 22 % of SIM@CACM microgel assembly remains after 15 days (Fig. S10), indicative of its good degradability *in vivo*.

The interconnected micropores within the SIM@CACM microgel assembly was confirmed by CLSM and SEM (Fig. S11). Moreover, cell adhesion and infiltration behaviors were also investigated by seeding BMSCs on the top surface of SIM@CACM microgel assembly and bulk hydrogel respectively (Fig. 3h). After 5 days of incubation, the number of BMSCs in the microgel assembly group was significantly higher than that in the hydrogel group (Fig. S12), possibly because the microgel assembly has higher specific surface area than hydrogel and thus promotes BMSC proliferation. More importantly, BMSCs don't infiltrate obviously into the hydrogel (Day 1: 20 ± 1.2 μm, Day 5: 37 ± 2.3 μm), although BMSCs on the surface of bulk hydrogel also increases. In contrast, BMSCs infiltrate significantly deeper into the microgel assembly (Day 1: 57 ± 3.3 μm, Day 5: 170 ± 5.2 μm), owing to the interconnected micropores inside SIM@CACM microgel assembly.

3.3. *In vitro chondrogenic differentiation*

In vitro chondrogenic differentiation of SIM@CACM microgel assembly was investigated via co-culture with BMSCs for 14 days. Clearly, BMSC proliferates much faster on CACM microgel assembly and SIM@CACM microgel assembly than CACM hydrogel, as proven by the DAPI staining in Fig. 4a and b. This phenomenon can be ascribed to the higher specific surface areas of CACM microgel assembly and SIM@CACM microgel assembly. F-actin staining reveals that BMSCs on CACM microgel assembly and SIM@CACM microgel assembly exhibit an organized spindle-shaped morphology and extended pseudopodia, whereas the actin filaments of BMSCs on CACM hydrogel scaffold show irregular aggregation, suggesting that both CACM microgel assembly and SIM@CACM microgel assembly can enhance cell adhesion and proliferation, while also maintain the morphology of cell filaments [53,54]. Immunofluorescence staining of Col II shows a significant increase in Col II expression in both SIM@CACM microgel assembly and CACM microgel assembly groups. It should be pointed out that no significant difference is observed between CACM microgel assembly and SIM@CACM microgel assembly in the terms of cell number, cell cytoskeleton morphology and Col II expression, proving that the addition of SIM into SIM@CACM microgel assembly and its sustained release don't affect the differentiation of BMSCs [55]. More importantly, considering the presence of blood in cartilage defect after microfracture operation, the above experiments were repeated again in blood-containing medium with the results shown in Fig. S13. No significant difference can be seen between regular medium and blood-containing medium, proving that blood does not negatively impact the chondrogenic differentiation of BMSCs on SIM@CACM microgel assembly.

Except bulky CACM hydrogel, *in vitro* chondrogenic differentiation performance of SIM@CACM microgel assembly was also compared with that of jammed SIM@CACM microgels and pure BMSCs spheroid. Rather than immunofluorescence staining of Col II, immunohistochemical staining of Col II and mRNA expression of Col2a1, Col1a1, Sox9, and aggrecan (ACAN) were performed to assess chondrogenic differentiation of BMSCs co-cultured with these three groups respectively for 4 weeks. The immunohistochemical staining images in Fig. 4c show that Col II expression in SIM@CACM microgel assembly group is higher than that in the SIM@CACM microgels group and pure BMSCs spheroid group. In the meantime, the mRNA expression in Fig. 4d shows that Col2a1, Col1a1, Sox9 and ACAN express significantly higher in the SIM@CACM microgel assembly group compared to the other two groups. Additionally, the expression of Col2a1 in the SIM@CACM microgel assembly group is much higher than that of Col1a1, indicating the formation of hyaline cartilage [56]. This suggests that the SIM@CACM microgel assembly can provide a favorable microenvironment for BMSCs to promote their chondrogenic differentiation into hyaline cartilage [57,58].

3.4. *In vivo BMSCs recruitment*

Prior to evaluating the long-term cartilage repair and regeneration of SIM@CACM microgel assembly, its BMSCs recruitment ability was first determined by injecting it into articular cartilage defect, retrieving the defect tissue after 5 days and staining for CD44 and CD90 via immunofluorescence [59,60]. Fig. 5a shows the immunofluorescence images of blank, CACM microgel assembly and SIM@CACM microgel assembly groups. The white horizontal line segments in these images indicate the boundary between cartilage and subchondral bone. As can be observed, the cell number above the white horizontal line segments in blank group is quite low, so do the CD44 and CD90 expression. This suggests the poor recruitment and residence of BMSCs in cartilage defect even after microfracture operation. In comparison, the attached cells as well as CD44 and CD90 expression increase notably after CACM microgel assembly is injected, which in our opinion proves the critical role of CACM microgel assembly in recruiting and anchoring BMSCs. More importantly, the release of SIM further enhances the BMSCs recruitment ability, as confirmed by the highest cell number, strongest CD44 and CD90 expression in SIM@CACM microgel assembly group. Fig. 5b illustrates the statistical analysis of the fluorescence intensity shown in Fig. 5a. Significant differences ($p < 0.01$ or 0.001) in CD44/CD90 expression and cell number can be seen among these three groups. These results demonstrate that SIM@CACM microgel assembly can effectively recruit and capture BMSCs in the early stage of cartilage repair, and thus offer enough seed cells for *in vivo* chondrogenic differentiation [61,62].

3.5. *In vivo cartilage repair and regeneration*

To further verify the cartilage repair and regeneration effects of SIM@CACM microgel assembly, *in vivo* animal test was carried out via articular cartilage defects in New Zealand rabbits. Four parallel samples including normal saline (blank control), SIM@CACM microgels, CACM microgel assembly and SIM@CACM microgel assembly were injected into the articular cartilage defects respectively after microfracture surgery (Fig. S14). Fig. 6 shows the optical images and H&E staining of articular cartilage defects after implanting the above four groups for 4 and 8 weeks. It can be found in Fig. 6a that the cartilage defects in the blank group and SIM@CACM microgels group are not completely filled with newborn cartilage after 4 weeks whilst the newborn cartilage in the CACM microgel assembly and SIM@CACM microgel assembly groups almost fill the cartilage defects. Part of the unassembled SIM@CACM microgels are missing in the second group mainly due to the lack of tissue adhesion, leading to the newborn cartilage in this group does not completely fill the defect. In addition, the integration degrees between the newborn cartilage and the surrounding original cartilage in the first two groups are lower than those of the last two groups. After implantation for 8 weeks, the newborn cartilage in the SIM@CACM microgel assembly group is quite transparent and shiny, and also shows excellent integration with the original cartilage (Fig. 6b). In contrast, the newborn cartilage color in the other three groups is only partially similar to that of the original cartilage and there are obvious wear and ivory fibrocartilage tissues [63].

Furthermore, the H&E staining results in Fig. 6a show that the newborn cartilage fibers in the blank group and SIM@CACM microgels group are arranged horizontally in week 4, indicative of a tendency towards fibrosis [64]. Compared with CACM microgel assembly group,

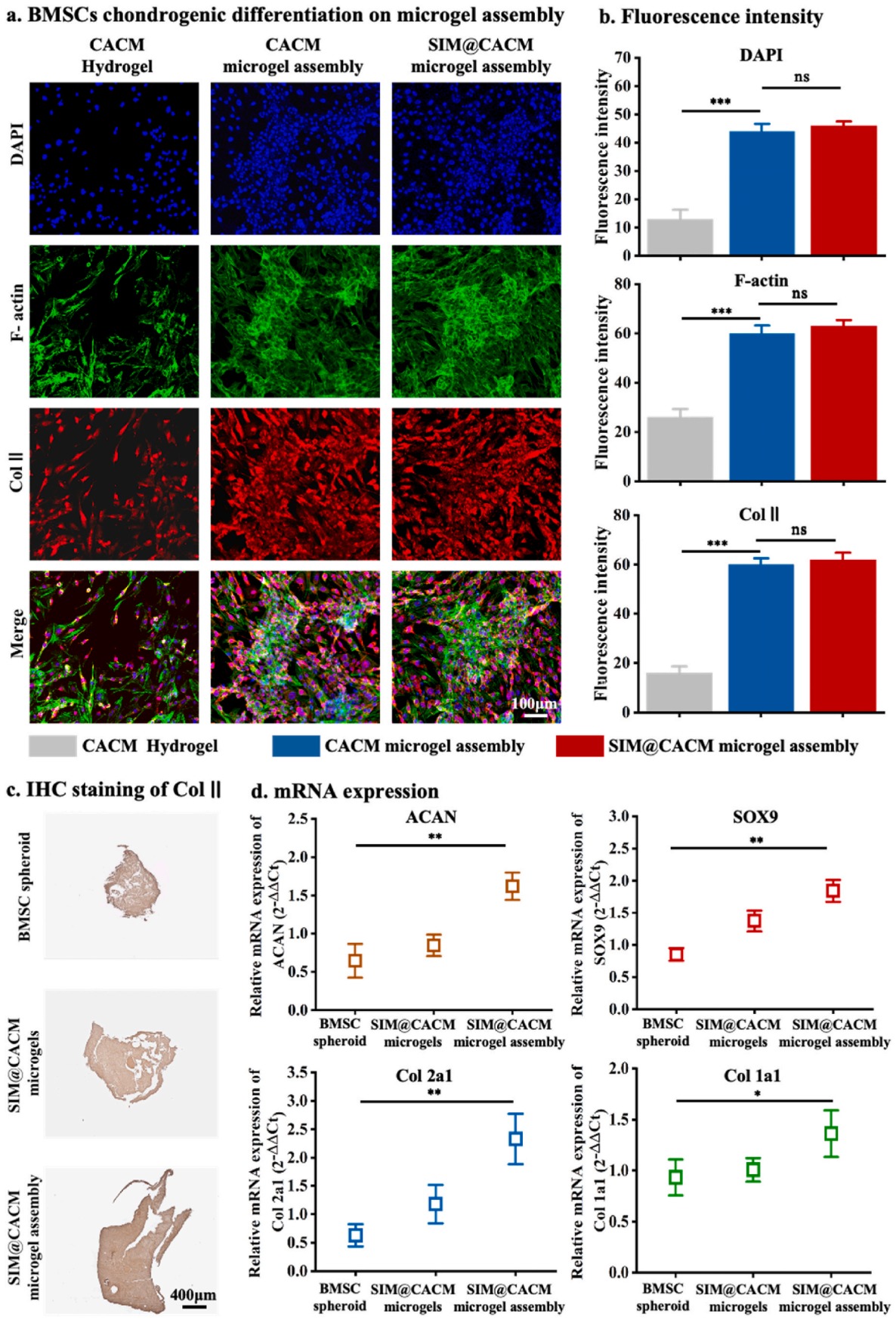

Fig. 4. *In vitro* chondrogenic differentiation of BMSCs cultured on SIM@CACM microgel assembly: a) fluorescence images of DAPI, F-actin and Col II; b) fluorescence intensities of DAPI, F-actin and Col II; c) immunohistochemical (IHC) staining of Col II; d) mRNA expression. ***P < 0.001, **P < 0.01, *P < 0.05, n = 4.

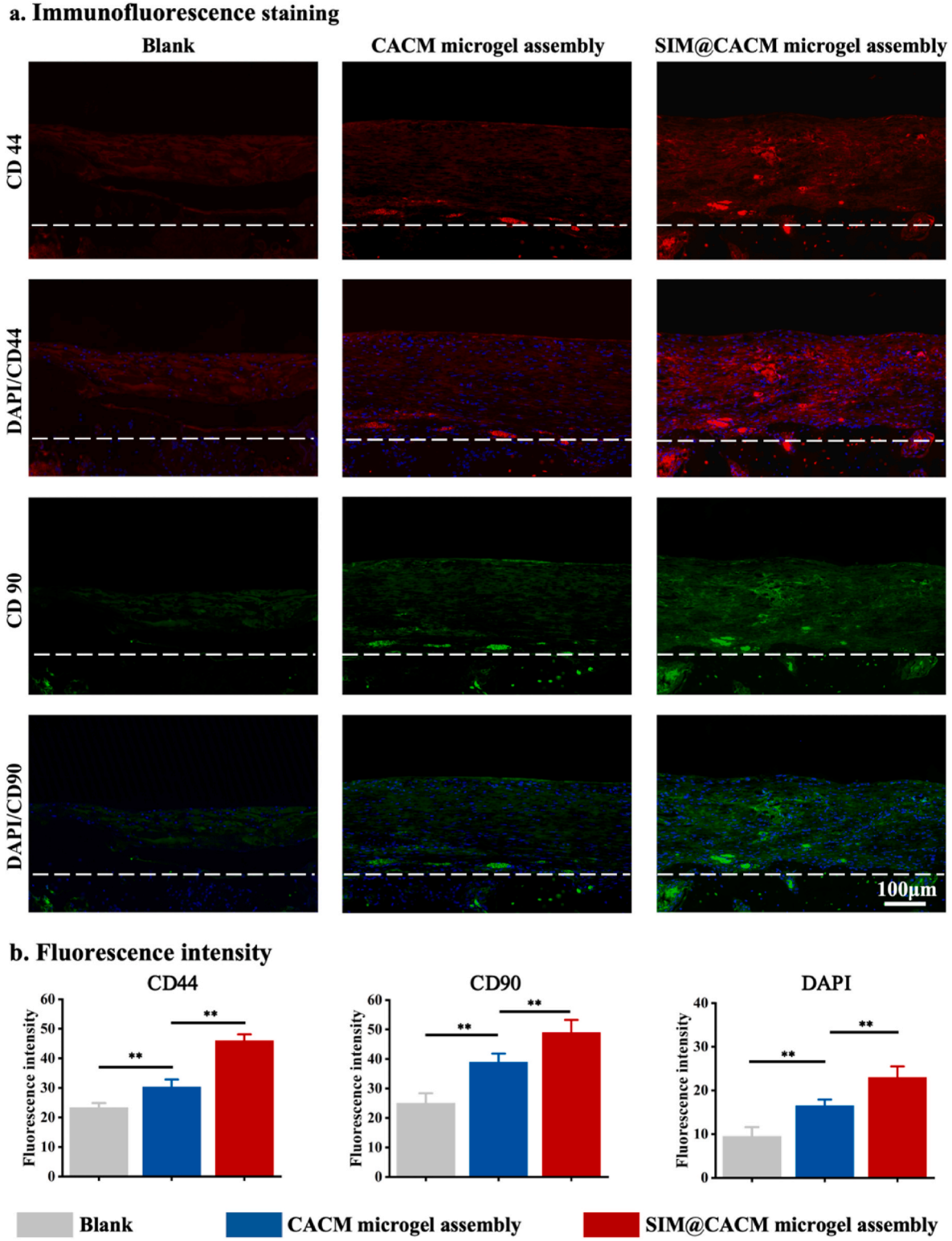

Fig. 5. *In vivo* BMSCs recruitment ability of SIM@CACM microgel assembly: a) fluorescence staining of DAPI, CD44 and CD90; b) statistical analysis of fluorescence intensity of CD44, CD90 and DAPI. ***P < 0.001, **P < 0.01, n = 4.

the cell number in SIM@CACM microgel assembly group is obviously higher, in agreement with its better BMSCs recruitment performance. Meanwhile, although the H&E staining images in Fig. 6b demonstrate that the newborn cartilages in the blank group and SIM@CACM microgels group completely fill the defect in week 8, their newborn cartilages are of low thickness and lack the normal orientation structure of chondrocytes. The newborn cartilage in the CACM microgel assembly group is thicker, but the interface between newborn cartilage and original cartilage is not very good, possibly due to insufficient BMSCs in the early stage of cartilage reconstruction that undergo uneven stress during movement. It is encouraging that the newborn cartilage in the SIM@CACM microgel assembly group is well integrated with the

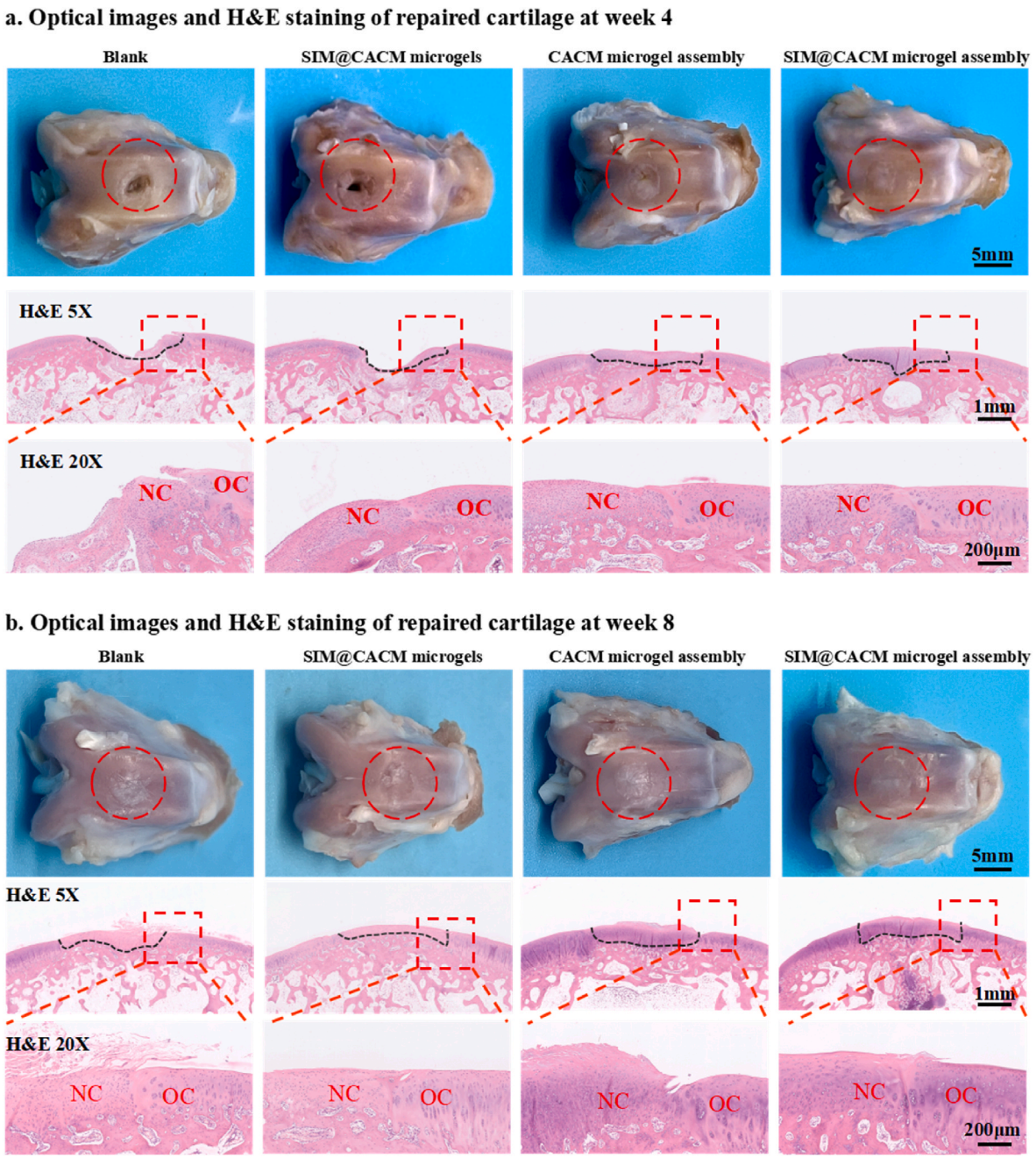

Fig. 6. Optical images and H&E staining of repaired cartilage after implanting normal saline, SIM@CACM microgels, CACM microgel assembly and SIM@CACM microgel assembly respectively for 4 and 8 weeks: a) optical images and H&E staining of repaired cartilage in week 4; b) optical images and H&E staining of repaired cartilage in week 8. NC stands for newborn cartilage, and OC stands for original cartilage. The black dotted line represents the interface between cartilage and subchondral bone in repaired cartilage. The color of the joint specimens appears darker because the specimen was fixed with 4 % paraformaldehyde before being photographed.

surrounding original cartilage, and its thickness is similar to that of original cartilage without obvious wear and fibrosis.

In addition to H&E staining, safranin O-fast green staining and immunohistochemical staining of Col II were further used to figure out their histological differences. The safranin O-fast green staining in Fig. 7a and Fig. S15a show that although the newborn cartilage in blank group and SIM@CACM microgels group fills the cartilage defects to a large extent after 8 weeks, the weak red color of the newborn cartilage in these two groups means the formation of fibrocartilage instead of hyaline cartilage. On the contrary, the strong red colors of the newborn cartilage matrix in CACM microgel assembly and SIM@CACM microgel assembly groups proves the presence of hyaline cartilage [65]. However, the surface of newborn hyaline cartilage of CACM microgel assembly is covered by a fibrocartilage layer. Besides, there are white voids existing inside the newborn cartilage matrix of CACM microgel assembly, indicating that the matrix is loose. Importantly, the newborn cartilage in SIM@CACM microgel assembly group exhibits the most similarity to the original cartilage, and the vertical orientation of cells is very obvious. As shown in Fig. 7b and Fig. S15b, the expressions of Col II in blank group and SIM@CACM microgels group are quite low in week 4. The obvious Col II expression as early as week 4 in SIM@CACM microgel assembly group indicates the *in vivo* chondrogenic differentiation of the recruited BMSCs towards hyaline cartilage occurs rapidly, owing to the favorable surrounding microenvironment. In week 8, the expression of Col II in the

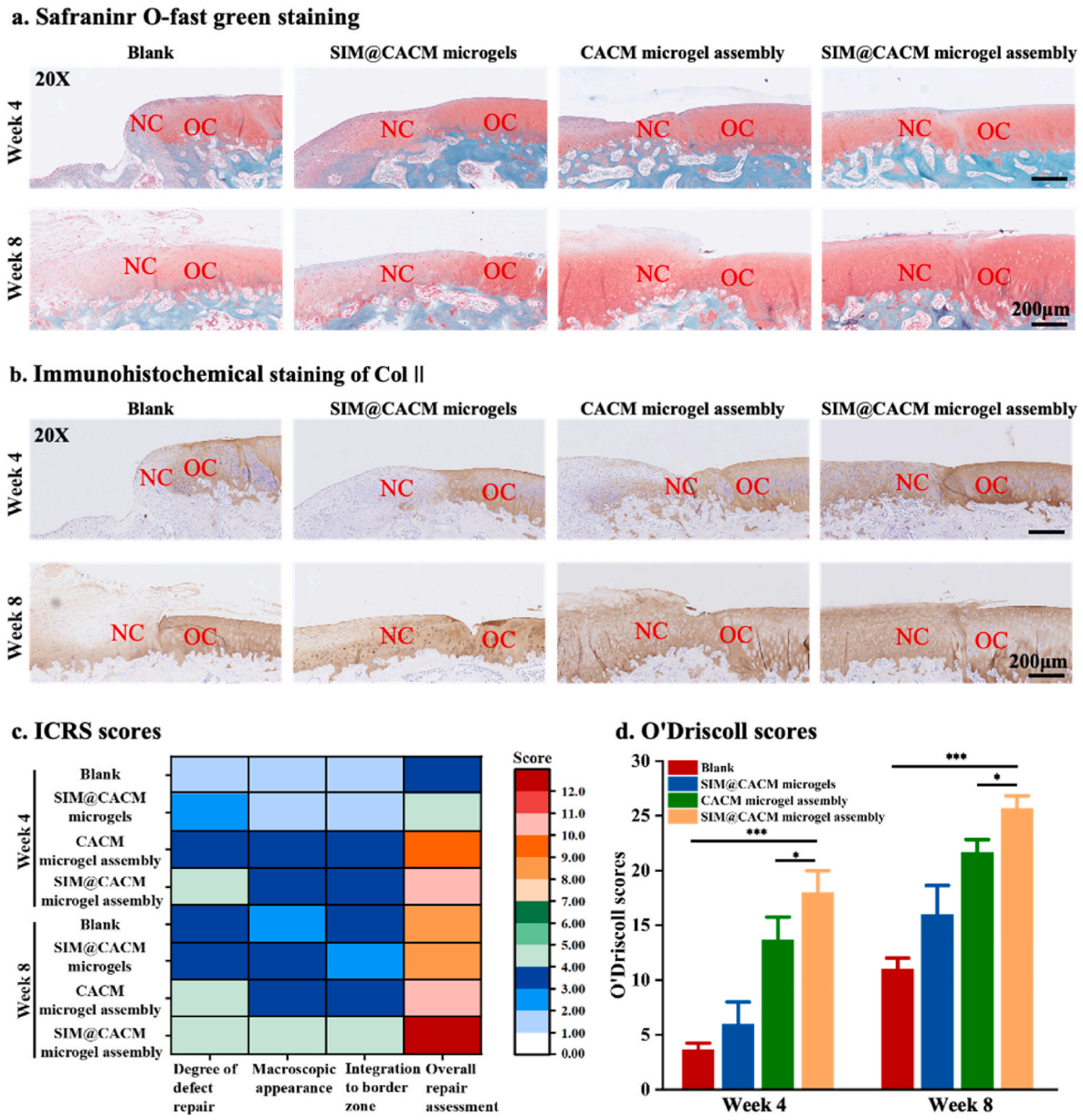

Fig. 7. a) Safranin O-fast green staining and b) immunohistochemical staining of Col II after implanting normal saline (blank), SIM@CACM microgels, CACM microgel assembly and SIM@CACM microgel assembly respectively for 4 and 8 weeks; c) evaluation of cartilage repair performance via ICRS scoring system; d) evaluation of cartilage repair performance via O'Driscoll scoring system; NC stands for newborn cartilage, and OC stands for original cartilage.

blank group is significantly lower than that in the other three groups, in good accordance with the bad long-term treatment effect of micro-fracture in clinic [66]. In SIM@CACM microgels group, the weak compressive strength of the new cartilage leads to fibrosis of the upper cartilage layer and low Col II expression. This situation is improved in CACM microgel assembly group and SIM@CACM microgel assembly group, i.e., the newborn hyaline cartilage layer becomes thicker. This is possibly caused by the fact that the microgel assembly can offer better mechanical cues than unassembled SIM@CACM microgels.

Finally, ICRS scoring system and O'Driscoll scoring system were also used by three observers to blindly score the efficiency of cartilage repair and regeneration (Tables S2 and S3). It can be seen from ICRS scores in Fig. 7c that the blank and SIM@CACM microgels groups show low scores in terms of the degree of defect repair, macroscopic appearance and the integration to border zone in week 4, whilst CACM microgel assembly and SIM@CACM microgel assembly obtain higher scores in these three aspects. In week 8, scores of all four groups increase, implying that all the four groups have certain degrees of cartilage repair effects regardless of newborn hyaline cartilage or fibrocartilage. Even introducing more complicated scoring criteria including safranin O staining and Col II staining etc, O'Driscoll scores in Fig. 7d still show that the cartilage repair performance of the above-mentioned four groups in descending order is SIM@CACM microgel assembly, CACM microgel assembly, SIM@CACM microgels and blank groups, which is also coincident with the results of ICRS scoring system.

The *in vivo* animal test shows that the newborn cartilage in the blank group and SIM@CACM microgels group display a tendency of fibrosis [67,68]. Although the cartilage repair in CACM microgel assembly group is better than that of blank group and SIM@CACM microgels group, the as-formed newborn cartilage looks like a hybrid of hyaline cartilage and fibrocartilage. Noteworthily, the differentiation of recruited BMSCs in SIM@CACM microgel assembly group into hyaline cartilage is the most obvious and the newborn cartilage is very close to the native cartilage in terms of structure and extracellular matrix

composition [69]. The progressive improvement in cartilage repair and regeneration from SIM@CACM microgels, CACM microgel assembly to SIM@CACM microgel assembly in comparison to the blank group (or namely, microfracture-based cartilage repair) fully validates the synergistic effects of several key factors. These include BMSCs recruitment (induced by SIM release from SIM@CACM microgels), bioactive factors (provided by the CACM matrix), appropriate mechanical strength (supplied by the microgel assembly), strong tissue adhesion (conferred by the OSA assembling agent), enhanced cell adhesion, proliferation and infiltration (facilitated by the interconnected micropores and high specific surface area of the microgels). Notably, the robust tissue adhesion ensures retention of SIM@CACM microgel assembly in the cartilage defect post-injection, while the sustained SIM release effectively recruits sufficient BMSCs from the bone marrow cavity in the early stages. The interconnected micropores and high surface area support rapid BMSC adhesion, proliferation and infiltration. Additionally, the bioactive factors within the CACM matrix, along with the mechanical stimuli provided by the microgel assembly, serve as biochemical and biophysical cues that promote the chondrogenic differentiation of BMSCs into hyaline cartilage.

4. Conclusion

In summary, a novel injectable SIM@CACM microgel assembly with BMSC recruitment and chondrogenic differentiation functions is constructed to improve microfracture-based articular cartilage regeneration. CACM is prepared via a modified extraction procedure and SIM@CACM microgels are then generated through water-in-oil emulsion method. The as-prepared microgels are assembled into SIM@CACM microgel assembly via dynamic Schiff base bonds after addition of OSA. Physiochemical characterization reveals that the SIM@CACM microgel assembly exhibit excellent injectability, tissue adhesion and appropriate mechanical modulus, while cytological characterization proves that BMSCs can adhere, proliferate and infiltrate rapidly in the SIM@CACM microgel assembly. *In vitro* chondrogenic differentiation experiments demonstrate that that SIM@CACM microgel assembly can induce the chondrogenic differentiation BMSCs into hyaline cartilage, as proven by the results of immunofluorescence staining, immunohistochemical staining and mRNA expression. *In vivo* studies demonstrate efficient early-stage BMSC recruitment and typical articular cartilage characteristics in newly formed tissue following injection into a rabbit cartilage defect. This favorable cartilage repair performance can be attributed to the unique structure and properties (good tissue adhesion, critical active factors, suitable mechanical strength, high specific surface area, abundant interconnected micropores) of the SIM@CACM microgel assembly and sustained SIM release to recruit autologous BMSCs, which creates an optimal biophysical and biochemical microenvironment for BMSCs to form hyaline cartilage. We believe that the SIM@CACM microgel assembly can overcome the current challenges of microfracture-based articular cartilage regeneration, and the relevant fabrication strategy may also offer a promising solution to other tissue engineering and regenerative medicine areas.

Ethics approval and consent to participate

All animal experiments were approved by the Animal Experimentation Centre of the South China University of Technology in accordance with the Regulations on the Administration of Laboratory Animals.

CRediT authorship contribution statement

Junlin Chen: Writing – original draft, Methodology, Investigation, Formal analysis, Data curation, Conceptualization. **Qingtao Li:** Methodology, Investigation, Data curation, Conceptualization. **Haofei Li:** Methodology, Investigation. **Chuhan Lv:** Methodology, Formal analysis. **Hongbo Yu:** Visualization, Data curation. **Qi Feng:** Supervision, Conceptualization. **Hua Dong:** Writing – review & editing, Supervision, Funding acquisition, Formal analysis, Conceptualization.

Declaration of competing interest

The authors declare that they have no known competing financial interests or personal relationships that could have appeared to influence the work reported in this paper.

Acknowledgements

This work was financially sponsored by the Key Research and Development Program of Guangdong Province (2023B0909020003), and the National Natural Science Foundation of China (Grant Nos. 52473130, 32071321).

Appendix A. Supplementary data

Supplementary data to this article can be found online at https://doi.org/10.1016/j.bioactmat.2024.10.013.

References

[1] W. Wei, Y. Ma, X. Yao, W. Zhou, X. Wang, C. Li, J. Lin, Q. He, S. Leptihn, H. Ouyang, Advanced hydrogels for the repair of cartilage defects and regeneration, Bioact. Mater. 6 (2021) 998.
[2] Y. Liu, L. Peng, L. Li, C. Huang, K. Shi, X. Meng, P. Wang, M. Wu, L. Li, H. Cao, K. Wu, Q. Zeng, H. Pan, 3D-bioprinted BMSC-laden biomimetic multiphasic scaffolds for efficient repair of osteochondral defects in an osteoarthritic rat model, Biomaterials 279 (2021) 121216.
[3] X. Pan, S. Yuan, Xiaojie Xun, Z. Fan, X. Xue, C. Zhang, J. Wang, J. Deng, Long-term recruitment of endogenous M2 macrophages by platelet lysate-rich plasma macroporous hydrogel scaffold for articular cartilage defect repair, Adv. Healthc. Mater. 11 (2022) 2101661.
[4] Z. Zhou, J. Cui, S. Wu, Z. Geng, J. Su, Silk fibroin-based biomaterials for cartilage/osteochondral repair, Theranostics 12 (2022) 5103–5124.
[5] Joseph A.M. Steele, A.C. Moore, Jean-Philippe St-Pierre, S.D. McCullen, A. J. Gormley, C.C. Horgan, Cameron RM. Black, C. Meinert, T. Klein, Siamak Saifzadeh, R. Steck, J. Ren, M.A. Woodruff, M.M. Stevens, In vitro and in vivo investigation of a zonal microstructured scaffold for osteochondral defect repair, Biomaterials 286 (2022) 121548.
[6] K. Abe, A. Yamashita, M. Morioka, Nanao Horike, Y. Takei, Saeko Koyamatsu, K. Okita, S. Matsuda, Noriyuki Tsumaki, Engraftment of allogeneic iPS cell-derived cartilage organoid in a primate model of articular cartilage defect, Nat. Commun. 14 (2023) 804.
[7] L. Zhou, Van Osch Gjvm, J. Malda, M.J. Stoddart, Y. Lai, R.Geoff Richards, Kevin Ki-Wai Ho, L. Qin, Innovative tissue-engineered strategies for osteochondral defect repair and regeneration: current progress and challenges, Adv. Healthc. Mater. 9 (2020) 2001008.
[8] J. Wu, Q. Chen, C. Deng, B. Xu, Z. Zhang, Y. Yang, T. Lu, Exquisite design of injectable hydrogels in cartilage repair, Theranostics 10 (2020) 9843–9864.
[9] T. Guo, Maeesha Noshin, H.B. Baker, Evin Taskoy, S.J. Meredith, Q. Tang, J. P. Ringel, M.J. Lerman, Y. Chen, J.D. Packer, J.P. Fisher, 3D printed biofunctionalized scaffolds for microfracture repair of cartilage defects, Biomaterials 185 (2018) 219–231.
[10] Z. Chen, T. Zhou, H. Luo, Z. Wang, Q. Wang, R. Shi, Z. Li, R. Pang, H. Tan, HWJMSC-EVs promote cartilage regeneration and repair via the ITGB1/TGF-β/Smad2/3 axis mediated by microfractures, J. Nanobiotechnol. 22 (2024) 117.
[11] A.R. Armiento, M. Alini, M.J. Stoddart, Articular fibrocartilage - why does hyaline cartilage fail to repair, Adv. Drug Deliver Rev. 146 (2019) 289–305.
[12] Z. Li, Y. Wang, C. Zhao, X. Li, M. Chen, Z. Liu, J. Liu, Y. Xiao, Y. Fan, Q. Jiang, Y. Sun, X. Zhang, Polysaccharide hybrid scaffold encapsulated endogenous factors for microfracture enhancement by sustainable release and cell recruitment, Compos Part B-Eng. 273 (2024) 111235.
[13] Z. Yang, H. Li, Z. Yuan, L. Fu, S. Jiang, C. Gao, F. Wang, Kangkang Zha, G. Tian, Z. Sun, B. Huang, F. Wei, F. Cao, X. Sui, J. Peng, S. Lu, W. Guo, S. Liu, Q. Guo, Endogenous cell recruitment strategy for articular cartilage regeneration, Acta Biomater. 114 (2020) 31–52.
[14] Y. Lei, Y. Wang, J. Shen, Z. Cai, Y. Zeng, P. Zhao, J. Liao, C. Lian, N. Hu, X. Luo, W. Cui, W. Huang, Stem cell-recruiting injectable microgels for repairing osteoarthritis, Adv. Funct. Mater. 31 (2021) 2105084.
[15] M. Wu, K. Zheng, W. Li, W. He, C. Qian, Z. Lin, H. Xiao, H. Yang, Y. Xu, M. Wei, J. Bai, D. Geng, Nature-inspired strategies for the treatment of osteoarthritis, Adv. Funct. Mater. 34 (2023) 2305603.
[16] W. Zakrzewski, Maciej Dobrzyński, M. Szymonowicz, Z. Rybak, Stem cells: past, present, and future, Stem Cell Res. Ther. 10 (2019) 68.
[17] O. Levy, Rui Kuai, Erika, Deepak Bhere, Y. Milton, Nabeel Nissar, Michael De Biasio, M. Heinelt, B. Reeve, R. Abdi, Meshael Alturki, Mohanad Fallatah,

Abdulaziz Almalik, A.H. Alhasan, K. Shah, J.M. Karp, Shattering barriers toward clinically meaningful MSC therapies, Sci. Adv. 6 (2020) eaba6884.
[18] N.A. Haq-Siddiqi, D. Britton, Jin Kim Montclare, Protein-engineered biomaterials for cartilage therapeutics and repair, Adv. Drug Deliv. Rev. 192 (2023) 114647.
[19] L. Zhu, Jieyu Yuhan, H. Yu, B. Zhang, K. Huang, L. Zhu, Decellularized extracellular matrix for remodeling bioengineering organoid's microenvironment, Small 19 (2023) 2207752.
[20] A.A. Golebiowska, J.T. Intravaia, V.M. Sathe, S.G. Kumbar, S.P. Nukavarapu, Decellularized extracellular matrix biomaterials for regenerative therapies: advances, challenges and clinical prospects, Bioact. Mater. 32 (2024) 98–123.
[21] H. Zhang, Y. Wang, Z. Zheng, X. Wei, L. Chen, Y. Wu, W. Huang, L. Yang, Strategies for improving the 3D printability of decellularized extracellular matrix bioink, Theranostics 13 (2023) 2562–2587.
[22] Y. Xu, L. Duan, Y. Li, Y. She, J. Zhu, G. Zhou, G. Jiang, Y. Yang, Nanofibrillar decellularized wharton's jelly matrix for segmental tracheal repair, Adv. Funct. Mater. 30 (2020) 1910067.
[23] Y. Ma, H. Shi, Q. Wei, Q. Deng, J. Sun, Z. Liu, B. Lai, G. Li, Y. Ding, W. Niu, Y. Zeng, X. Zeng, Developing a mechanically matched decellularized spinal cord scaffold for the in situ matrix-based neural repair of spinal cord injury, Biomaterials 279 (2021) 121192.
[24] Byoung Soo Kim, S. Das, J. Jang, D.-W. Cho, Decellularized extracellular matrix-based bioinks for engineering tissue- and organ-specific microenvironments, Chem. Rev. 120 (2020) 10608–10661.
[25] Y. Sun, L. Yan, S. Chen, M. Pei, Functionality of decellularized matrix in cartilage regeneration: a comparison of tissue versus cell sources, Acta Biomater. 74 (2018) 56–73.
[26] P. Guo, N. Jiang, C. Mini, Gregor Miklosic, S. Zhu, A. Vernengo, Matteo D'Este, S. Grad, M. Alini, Z. Li, Decellularized extracellular matrix particle-based biomaterials for cartilage repair applications, J. Mater. Sci. Technol. 160 (2023) 194–203.
[27] X. Zhang, X. Chen, H. Hong, R. Hu, J. Liu, C. Liu, Decellularized extracellular matrix scaffolds: recent trends and emerging strategies in tissue engineering, Bioact, Mater. 10 (2022) 15–31.
[28] Q. Feng, H. Gao, H. Wen, H. Huang, Q. Li, M. Liang, Y. Liu, H. Dong, X. Cao, Engineering the cellular mechanical microenvironment to regulate stem cell chondrogenesis: insights from a microgel model, Acta Biomater. 113 (2020) 393–406.
[29] Q. Feng, Q. Li, H. Wen, J. Chen, M. Liang, H. Huang, D. Lan, H. Dong, X. Cao, Injection and self-assembly of bioinspired stem cell-laden gelatin/hyaluronic acid hybrid microgels promote cartilage repair in vivo, Adv. Funct. Mater. 29 (2019) 1906690.
[30] H. Huang, Y. Shang, H. Li, Q. Feng, Y. Liu, J. Chen, H. Dong, Co-transplantation of islets-laden microgels and biodegradable O_2-generating microspheres for diabetes treatment, ACS Appl. Mater. Interfaces 14 (2022) 38448.
[31] Q. Feng, D. Li, Q. Li, H. Li, Z. Wang, S. Shuang, Z. Lin, X. Cao, H. Dong, Assembling microgels via dynamic cross-linking reaction improves printability, microporosity, tissue-adhesion, and self-healing of microgel bioink for extrusion bioprinting, ACS Appl. Mater. Interfaces 14 (2022) 15653.
[32] Q. Feng, D. Li, Q. Li, S. Li, H. Huang, H. Li, H. Dong, X. Cao, Dynamic nanocomposite microgel assembly with microporosity, injectability, tissue-adhesion, and sustained drug release promotes articular cartilage repair and regeneration, Adv. Healthc. Mater. 11 (2021) 2102395.
[33] J. Wu, L. Fu, Z. Yan, Y. Yang, H. Yin, P. Li, X. Yuan, Z. Ding, T. Kang, Z. Tian, Z. Liao, G. Tian, C. Ning, Y. Li, X. Sui, M. Chen, S. Liu, Q. Guo, Hierarchical porous ECM scaffolds incorporating GDF-5 fabricated by cryogenic 3D printing to promote articular cartilage regeneration, Biomate Res 27 (2023) 7.
[34] J. Lu, X. Shen, X. Sun, H. Yin, S. Yang, C. Lu, Y. Wang, Y. Liu, Y. Huang, Z. Yang, X. Dong, C. Wang, Q. Guo, L. Zhao, X. Sun, S. Lu, A.G. Mikos, J. Peng, X. Wang, Increased recruitment of endogenous stem cells and chondrogenic differentiation by a composite scaffold containing bone marrow homing peptide for cartilage regeneration, Theranostics 8 (2018) 5039–5058.
[35] Bhavana Mohanraj, G. Duan, A. Peredo, M. Kim, F. Tu, D. Lee, G.R. Dodge, R. L. Mauck, Mechanically activated microcapsules for "on-demand" Drug delivery in dynamically loaded musculoskeletal tissues, Adv. Funct. Mater. 29 (2019) 1807909.
[36] D. Zhou, X. Yan, L. Xiao, J. Wang, J. Wei, Gold capped mesoporous bioactive glass guides bone regeneration via BMSCs recruitment and drug adaptive release, Chem. Eng. J. 487 (2024) 150546.
[37] Z. Wan, Q. Dong, Y. Liu, X. Zhang, P. Zhang, Longwei Lv, Y. Zhou, Programmed biomolecule delivery orchestrate bone tissue regeneration via MSC recruitment and epigenetic modulation, Chem. Eng. J. 438 (2022) 135518.
[38] T. He, C. Zhang, Armin Vedadghavami, S. Mehta, H.A. Clark, R.M. Porter, A. G. Bajpayee, Multi-arm Avidin nano-construct for intra-cartilage delivery of small molecule drugs, J. Control. Release. 318 (2020) 109–123.
[39] Z. Zhao, X. Xia, J. Liu, M. Hou, Y. Liu, Z. Zhou, Y. Xu, F. He, H. Yang, Y. Zhang, C. Ruan, X. Zhu, Cartilage-inspired self-assembly glycopeptide hydrogels for cartilage regeneration via ROS scavenging, Bioact. Mater. 32 (2024) 319–332.
[40] H. Huang, J. Li, C. Wang, L. Xing, H. Cao, C. Wang, Chung Yan Leung, Z. Li, Y. Xi, H. Tian, F. Li, D. Sun, Using decellularized magnetic microrobots to deliver functional cells for cartilage regeneration, Small 20 (2023) 2304088.
[41] M. Akita, Y. Nishikawa, Yuya Shigenobu, Daisuke Ambe, T. Morita, K. Morioka, K. Adachi, Correlation of proline, hydroxyproline and serine content, denaturation temperature and circular dichroism analysis of type I collagen with the physiological temperature of marine teleosts, Food Chem. 329 (2020) 126775.
[42] Navatha Shree Sharma, A. Karan, Huy Quang Tran, J.V. John, Syed Muntazir Andrabi, S.M. Shatil Shahriar, J. Xie, Decellularized extracellular matrix-decorated 3d nanofiber scaffolds enhance cellular responses and tissue regeneration, Acta Biomater. 184 (2024) 81–97.
[43] L. Jia, P. Zhang, Z. Ci, X. Hao, B. Bai, W. Zhang, H. Jiang, G. Zhou, Acellular cartilage matrix biomimetic scaffold with immediate enrichment of autologous bone marrow mononuclear cells to repair articular cartilage defects, Mater Today Bio 15 (2022) 100310.
[44] H. Wen, J. Li, G.L. Payne, Q. Feng, M. Liang, J. Chen, H. Dong, X. Cao, Hierarchical patterning via dynamic sacrificial printing of stimuli-responsive hydrogels, Biofabrication 12 (2020) 035007.
[45] Y. Li, L. Li, M. Wang, B. Yang, B. Huang, S. Bai, X. Zhang, N. Hou, H. Wang, Z. Yang, C. Tang, Y. Li, Wayne Yuk-Wai Lee, L. Feng, M.D. Tortorella, G. Li, O-alg-THAM/gel hydrogels functionalized with engineered microspheres based on mesenchymal stem cell secretion recruit endogenous stem cells for cartilage repair, Bioact. Mater. 28 (2023) 255–272.
[46] X. Xu, H. Li, J. Chen, Chuhan Lv, W. He, X. Zhang, Q. Feng, H. Dong, A universal strategy to construct high-performance homo- and heterogeneous microgel assembly bioinks, Small Methods (2024) 2400223.
[47] L. Lian, M. Xie, Z. Luo, Z. Zhang, Sushila Maharjan, X. Mu, Carlos Ezio Garciamendez-Mijares, X. Kuang, Jugal Kishore Sahoo, G. Tang, G. Li, D. Wang, J. Guo, Federico Zertuche González, V. Manjarrez, L. Cai, X. Mei, D.L. Kaplan, YuShrike Zhang, Rapid volumetric bioprinting of decellularized extracellular matrix bioinks, Adv. Mater. 36 (2024) 2304846.
[48] L. Xin, X. Zheng, J. Chen, S. Hu, Y. Luo, Q. Ge, X. Jin, L. Ma, S. Zhang, An acellular scaffold facilitates endometrial regeneration and fertility restoration via recruiting endogenous mesenchymal stem cells, Adv. Healthc. Mater. 11 (2022) 2201680.
[49] W. Sun, Y. Yang, L. Wang, H. Tang, L. Zhang, Y. She, X. Xiao, X. Hu, Q. Feng, C. Chen, Utilization of an acellular cartilage matrix-based photocrosslinking hydrogel for tracheal cartilage regeneration and circumferential tracheal repair, Adv. Funct. Mater. 32 (2022) 2201257.
[50] W. He, H. Li, X. Xu, X. Zhang, J. Chen, Chuhan Lv, H. Yu, Q. Feng, H. Dong, An injectable and retrievable bioartificial pancreas fabricated by time-sequentially assembling islets-laden microgels for minimally invasive treatment of type 1 diabetes, Chem. Eng. J. 492 (2024) 152261.
[51] H. Li, Y. Shang, Q. Feng, Y. Liu, J. Chen, H. Dong, A novel bioartificial pancreas fabricated via islets microencapsulation in anti-adhesive core-shell microgels and macroencapsulation in a hydrogel scaffold prevascularized in vivo, Bioact. Mater. 27 (2023) 362–376.
[52] H. Jiang, C. Lou, L. Jiang, C. Lin, W. Wang, Z. Yan, J. Yu, T. Cai, S. Lin, J. Wang, X. Pan, X. Xue, Simvastatin-enhanced bioinspired exosome mimetics regulate osteogenesis and angiogenesis for the treatment of glucocorticoid-induced osteonecrosis of the femoral head, Chem. Eng. J. 472 (2023) 144729.
[53] A.J. Vernengo, S. Grad, D. Eglin, M. Alini, Z. Li, Bioprinting tissue analogues with decellularized extracellular matrix bioink for regeneration and tissue models of cartilage and intervertebral discs, Adv. Funct. Mater. 30 (2020) 1909044.
[54] X. Ji, Z. Lei, M. Yuan, H. Zhu, X. Yuan, W. Liu, H. Pu, J. Jiang, Y. Zhang, X. Jiang, J. Xiao, Cartilage repair mediated by thermosensitive photocrosslinkable TGFβ1-loaded GM-HPCH via immunomodulating macrophages, recruiting MSCs and promoting chondrogenesis, Theranostics 10 (2020) 2872–2887.
[55] B. Huang, P. Li, M. Chen, L. Peng, X. Luo, G. Tian, H. Wang, L. Wu, Q. Tian, H. Li, Y. Yang, S. Jiang, Z. Yang, Kangkang Zha, X. Sui, S. Liu, Q. Guo, Hydrogel composite scaffolds achieve recruitment and chondrogenesis in cartilage tissue engineering applications, J. Nanobiotechnol. 20 (2022) 25.
[56] Z. Zhou, P. Song, Y. Wu, M. Wang, C. Shen, Z. Ma, X. Ren, X. Wang, X. Chen, Y. Hu, Z. Li, Q. Zhang, M. Li, Z. Geng, J. Su, Dual-network DNA–silk fibroin hydrogels with controllable surface rigidity for regulating chondrogenic differentiation, Mater. Horiz. 11 (2024) 1465–1483.
[57] M. Chen, Y. Sun, Y. Hou, Z. Luo, M. Li, Y. Wei, M. Chen, L. Tan, K. Cai, Y. Hu, Constructions of ROS-responsive titanium-hydroxyapatite implant for mesenchymal stem cell recruitment in peri-implant space and bone formation in osteoporosis microenvironment, Bioact. Mater. 18 (2022) 56–71.
[58] W. Dai, X. Gong, C. Wang, P. Liu, W. Shi, J. Cheng, C. Cao, X. Hu, J. Wang, Y. Ao, Injectable decellularized extracellular matrix hydrogel with cell-adaptable supramolecular network enhances cartilage regeneration by regulating inflammation and facilitating chondrogenesis, Chem. Eng. J. 498 (2024) 155138.
[59] B. Cai, D. Lin, Y. Li, L. Wang, J. Xie, T. Dai, F. Liu, M. Tang, L. Tian, Y. Yuan, L. Kong, Steve, N2-polarized neutrophils guide bone mesenchymal stem cell recruitment and initiate bone regeneration: a missing piece of the bone regeneration puzzle, Adv. Sci. 8 (2021) 2100584.
[60] W. Sun, Y. Yang, L. Wang, H. Tang, L. Zhang, Y. She, X. Xiao, X. Hu, Q. Feng, C. Chen, Utilization of an acellular cartilage matrix-based photocrosslinking hydrogel for tracheal cartilage regeneration and circumferential tracheal repair, Adv. Funct. Mater. 32 (2022) 2201257.
[61] Y. Xu, L. Duan, Y. Li, Y. She, J. Zhu, G. Zhou, G. Jiang, Y. Yang, Nanofibrillar decellularized wharton's jelly matrix for segmental tracheal repair, Adv. Funct. Mater. 30 (2020) 1010067.
[62] X. Nie, Yon Jin Chuah, W. Zhu, P. He, Y. Peck, D.-A. Wang, Decellularized tissue engineered hyaline cartilage graft for articular cartilage repair, Biomaterials 235 (2020) 119821.
[63] C. Shen, J. Wang, G. Li, S. Hao, Y. Wu, P. Song, Y. Han, M. Li, G. Wang, K. Xu, H. Zhang, X. Ren, Y. Jing, R. Yang, Z. Geng, J. Su, Boosting cartilage repair with silk fibroin-DNA hydrogel-based cartilage organoid precursor, Bioact. Mater. 35 (2024) 429–444.
[64] Manivannan Sivaperuman Kalairaj, R. Pradhan, W. Saleem, M.M. Smith, A. K. Gaharwar, Intra-articular injectable biomaterials: therapeutic delivery for cartilage repair and regeneration, Adv. Healthc. Mater. (2024) 2303794.

[65] W. Gao, K. Chen, W. He, S. Zhao, D. Cui, C. Tao, Y. Xu, X. Xiao, Q. Feng, H. Xia, Synergistic chondrogenesis promotion and arthroscopic articular cartilage restoration via injectable dual-drug-loaded sulfated hyaluronic acid hydrogel for stem cell therapy, Compos Part B Eng 263 (2023) 110857.
[66] H. Wu, L. Shen, Z. Zhu, X. Luo, Y. Zhai, X. Hua, S. Zhao, L. Cen, Z. Zhang, A cell-free therapy for articular cartilage repair based on synergistic delivery of SDF-1 & KGN with HA injectable scaffold, Chem. Eng. J. 393 (2020) 124649.
[67] J. Wei, P. Ran, Q. Li, J. Lu, L. Zhao, Y. Liu, X. Li, Hierarchically structured injectable hydrogels with loaded cell spheroids for cartilage repairing and osteoarthritis treatment, Chem. Eng. J. 430 (2022) 132211.
[68] T. Lin, Y. Zhao, J. Chen, C. Wu, Z. Li, Y. Cao, R. Lu, J. Zhang, C. Zhao, Y. Lu, Carboxymethyl chitosan-assisted MnOx nanoparticles: synthesis, characterization, detection and cartilage repair in early osteoarthritis, Carbohyd. Polym. 294 (2022) 119821.
[69] T. Chen, N. Dai, T. Wen, S. Hsu, An acellular, self-healed trilayer cryogel for osteochondral regeneration in rabbits, Adv. Healthc. Mater. (2024) 2400462.